Journal of Materials Chemistry A

Precisely Segmented PEEK-Ionene + Ionic Liquid Composite Membranes for CO2 Separation

Journal:	*Journal of Materials Chemistry A*
Manuscript ID	TA-ART-08-2023-005223.R2
Article Type:	Paper
Date Submitted by the Author:	04-Dec-2023
Complete List of Authors:	Ravula, Sudhir; The University of Alabama, Chemical & Biological Engineering Chen, Ying; Pacific Northwest National Laboratory, Environmental Molecular Sciences Laboratory Wise, Kevin; The University of Alabama, Chemical & Biological Engineering Shinde, Pravin; The University of Alabama, Chemical & Biological Engineering Walter, Eric; Pacific Northwest National Laboratory, Environmental Molecular Sciences Laboratory Karkamkar, Abhi; PNNL, Catalysis Science Heldebrant, David; Pacific Northwest National Lab, Applied Synthetic Chemistry Bara, Jason; The University of Alabama, Chemical & Biological Engineering

ARTICLE

Precisely Segmented PEEK-Ionene + Ionic Liquid Composite Membranes for CO_2 Separation

Received 00th January 20xx,
Accepted 00th January 20xx

DOI: 10.1039/x0xx00000x

Sudhir Ravula,[a] Ying Chen,[b] Kevin W. Wise[a], Pravin S. Shinde,[a] Eric D. Walter,[c] Abhi Karkamkar,[c] David J. Heldebrant[d, e] and Jason E. Bara*[a]

Ionenes, polymers with ionic groups incorporated directly within the backbone are a highly versatile class of materials, although they have received much less attention than polyelectrolytes which have ionic groups pendant from the polymer backbone. By designing ionenes that incorporate robust properties of poly(ether ether ketone) (PEEK), we have achieved new imidazolium-containing PEEK-ionene architectures that create opportunities for enhanced CO_2 separation membranes. To achieve these materials, an new imidazole-functionalized PEEK oligomer (ImK(EEK)$_2$KIm) was synthesized through facile and straightforward routes. This molecule was then polymerized via condensation reactions with two different aromatic (α,α′-dibromo-*p*-xylene) and aliphatic (dibromohexyl containing-bis(imidazolium)hexane dibromide salt) comonomers and exchanged with bistriflimide ([Tf_2N]) anion to obtain two unique PEEK-ionenes containing distinct PEEK and ionic segments: *p*([ImK(EEK)$_2$Im-*p*-xyl][Tf_2N]$_2$) and *p*([ImK(EEK)$_2$(ImC_6)$_3$][Tf_2N]$_4$). While the neat PEEK-ionenes exhibited high molecular weight but were not able to form high-quality films, adding stoichiometric amounts of "free" IL (1-methyl-3-butylimidazolium bistriflimide, [C_4mIm][Tf_2N]), greatly improved the flexibility and processeability of the resultant membranes. Further, the structure–property relationships of bulk PEEK-ionenes and corresponding composites were extensively characterized by different analytical techniques (thermogravimetric analysis, differential scanning calorimetry, X-ray diffraction, and solid-state NMR). The gas separation properties were investigated, with the PEEK-ionenes + IL composites exhibiting CO_2 permeabilities of 14–94 barrer and good CO_2/N_2 permselectivities of 26–35, indicating that new designs of segmented ionenes and composites with ILs a promising material design strategy for developing gas separation membranes.

Introduction

Over the years, human beings have been the primary contributors for the release of greenhouse gases, in particular CO_2, from the combustion of fossil fuels. This has resulted in climatic changes in the earth's atmosphere, causing mankind to face both economic and environmental challenges.[1, 2] Separation of CO_2 from other gases (especially CH_4 or H_2) in various processes is a key component of many industrial processes. Recent emphasis has been on the separation of CO_2 from N_2 given the need to capture CO_2 from post-combustion sources as well through direct air capture (DAC). Membrane separation technologies offer low-energy consumption, minimal process footprint, and cost-effectiveness relative to conventional technologies applied in industrial processes such as the recovery of H_2 in the production of NH_3, the production of N_2 gas from the air, and removal of CO_2 from the flue gas, and natural gas sweetening.[3-5] Toward this, diverse polymeric membrane-based gas separations are extensively studied in industrial and academic labs, but only a handful of polymers have achieved commercial success. The performance of polymeric membranes for gas separations is commonly evaluated in terms of permeability and selectivity parameters. However, a strong trade-off generally exists between permeability and selectivity, effectively depicted through Robeson's upper-bound correlations for common gas pairs.[6, 7] Thus, the development of high-performance polymeric membranes with high permeability and selectivity, improved processability, as well as chemical and thermal stability, is a goal of most current research.

Poly(aryl ether ketones) (collectively, PAEK) are a family of high-performance (HP) engineering thermoplastics, which have received significant commercial attention for their semi-crystalline character and outstanding physicochemical properties.[8, 9] Among these polymers, poly(ether ether ketone) (PEEK) is the most widely used material, exhibiting a glass transition temperature (T_g) of 145 °C and a high melting point (T_m) of ~340 °C, as well as high mechanical strength, excellent thermal stability, and good chemical resistance. The robust properties of PEEK would seemingly make it an ideal candidate

[a] *University of Alabama, Department of Chemical & Biological Engineering, Tuscaloosa, AL 35487-0203 USA*
[b] *Physical and Computational Sciences Directorate, Pacific Northwest National Laboratory, Richland, WA 99352 USA*
[c] *Environmental Molecular Sciences Laboratory, Pacific Northwest National Laboratory, Richland, WA 99352 USA*
[d] *Energy and Environment Directorate, Pacific Northwest National Laboratory, Richland, WA 99352 USA*
[e] *Washington State University, Department of Chemical Engineering and Bioengineering, Pullman, WA 99163 USA*
† Footnotes relating to the title and/or authors should appear here.
Electronic Supplementary Information (ESI) available: [details of any supplementary information available should be included here]. See DOI: 10.1039/x0xx00000x

for gas separation membranes. Unfortunately, pristine PEEK and functionalized PEEK materials exhibit low CO_2 permeabilities (0.96–19.4) with CO_2/N_2 permselectivity of 20–24.[10, 11] Further, it is difficult to process PEEK materials into thin membranes/films due to their poor solubility in common organic solvents. Due to a high tendency toward crystallization and limited solubility, structural modifications to the PEEK backbone are generally limited to nitration and sulfonation, or introduction benzylic halides, etc.[12, 13] The solubility of modified PEEK materials is generally greatly increased and this is advantageously utilized in wide variety of applications including solid polymer electrolytes, ion-exchange membranes, fuel cells, gas separation membranes, and antimicrobial coatings.[13-15] Similar approaches have also been applied to poly(ethersulfone) materials. For instance, Chung *et al.* examined the sulfonated PES (SPES) membranes for CO_2 separation, which displayed lower permeability and increased permselectivity as the degree of sulfonation increased.[16] Additionally, SPES membranes are fabricated with transition metals through ion-exchange treatment and found that Zn-form membranes showed improved selectivity compared with SPES membranes. As a result, significant efforts have been devoted by researchers to synthesize sulfonated PEEK membranes, along with other embedded functional moieties (e.g., —COOH, —NH_2, and —F) and bulky groups which increase fractional free volume (FFV) to improve the CO_2 permeation and separation performance.[17-20] The strong affinity of functional groups toward the quadrupolar CO_2 molecules might enhance the CO_2 solubility selectivity of PEEK membranes. Nevertheless, the introduction of CO_2-philic groups in polymeric membranes is mainly limited to post-modification, which reduces the tendency to crystallize, decreases the mechanical strength, and reduces the chemical resistance of PEEK polymers.

Ionic polymers have emerged as promising materials within membrane science due to their processability and a general affinity towards polar molecules (i.e., CO_2) when compared to non-ionic polymers. Based on the location of the ions (which are typically cations), ionic polymers are classified into two groups. Polyelectrolytes are generally synthesized via the polymerization of ionic monomers (e.g., styrenes, acrylates) and as a result have ionic (cationic) groups at the pendant of each repeating unit.[21, 22] Polymerized ionic liquids (poly(ILs)) are a subset of polyelectrolytes. Imidazolium cations can also be introduced as pendants to the aromatic rings of polymers such as PEEK, PAEK, poly(2,6-dimethyl-1,4-phenyleneoxide), polyfluorene, and fluorinated poly(aryl ether oxadiazole)s are extensively explored as proton-conduction membranes for fuel cell applications.[23-28] Generally, these cationic polyelectrolyte forms of PEEK have been synthesized via benzylic bromination with *N*-bromosuccinimide, and subsequent quaternization using imidazoles or amines. Recently, Kammakakam, *et al.* demonstrated the imidazolium-functionalized PEEK (Im-PEEK) polyelectrolyte with different alkyl chain lengths.[29] The presence of flexible alkyl chains in the Im-PEEK polyelectrolytes reduced the FFV of the polymers, which resulted in reduced permeability but showed enhanced O_2/N_2 permselectivity of 15.5.

On the other hand, ionenes are polymers where the ions (again, typically cations) are embedded within the polymeric backbone,[30, 31] and are becoming of increasing interest for gas separation membranes and other applications. For instance, Piron *et al.* blended benzimidazolium ionenes with diphenyl-ether linked poly(benzimidazole) to prepare self-supporting membranes for a vanadium redox flow battery application.[32] Further, Thankamony *et al.* reported gel polymer electrolyte prepared from poly(ethylene oxide)-based (PEO) imidazolium ionene blended with poly(vinylidene fluoride-hexafluoropropylene) support and lithium bistriflimide ($LiTf_2N$) salt for Li-ion batteries.[33] Subsequently, Kammakakam e*t al.* extended the later work by crosslinking the diacrylate monomer with PEO containing imidazolium ionene to form a mechanically stable membrane for efficient CO_2/N_2 separation (33.5).[34] Overall, a handful of reports in the literature have studied the properties of both neat and ion-containing PEEK polymers as gas separation membranes.

Recently, our group has been developing ultra-high-performance (UHP) and HP ionenes and studied their use as CO_2-selective polymer membranes. For instance, we developed imidazolium-containing polyimide ionenes (PI-ionenes) by polymerizing a bisimidazole diimide monomer "PMDA-API" with xylyl linkages attached at different positions (ortho-, meta-, and para-) via the Menshutkin reaction.[35] These materials have greatly improved thermal and mechanical properties compared to "simple" ionenes where the cations are linked by alkyl chains. Interestingly, the permeabilities of these PI-ionenes improved considerably after soaking in $[C_4mIm][Tf_2N]$ IL which had absorbed into the PI-ionene. Similarly, we successfully incorporated Troger's base (TB) groups into imidazolium ionenes and the resultant materials exhibited an excellent CO_2/CH_4 permselectivity of 82.5.[36]

Overall, the presence of ionic groups in the main-chain polymers yield high-quality membranes that displayed promising CO_2 separation properties. Currently, our group is interested in the synergistic interaction of ionenes and PEEK polymer to better understand the influence of each component on ionene solubility, processability, thermal/mechanical properties, and gas separation performance. Towards this, we reported new class of imidazolium PEEK ionenes for gas separation membranes.[37] The CO_2 permeability was enhanced 4x when compared to neutral PEEK membrane indicating the influence of ionic groups within the polymeric backbone. Further, incorporation of distinct kinds of free IL into the PEEK ionene matrix resulted in different gas transport properties, suggesting the IL impregnation greatly impacts the molecular interactions with the ionenes. However, while the performance of PEEK ionenes is below the Robeson bound, this initial proof of concept is promising and provides a roadmap by which to develop PEEK-ionenes as gas separation membranes, especially by lengthening both the PEEK and ionic segments.

Towards this goal we have examined prior works in the synthesis of PEEK oligomers of precise length. The foundation of these methods comes from Jonas and co-workers who

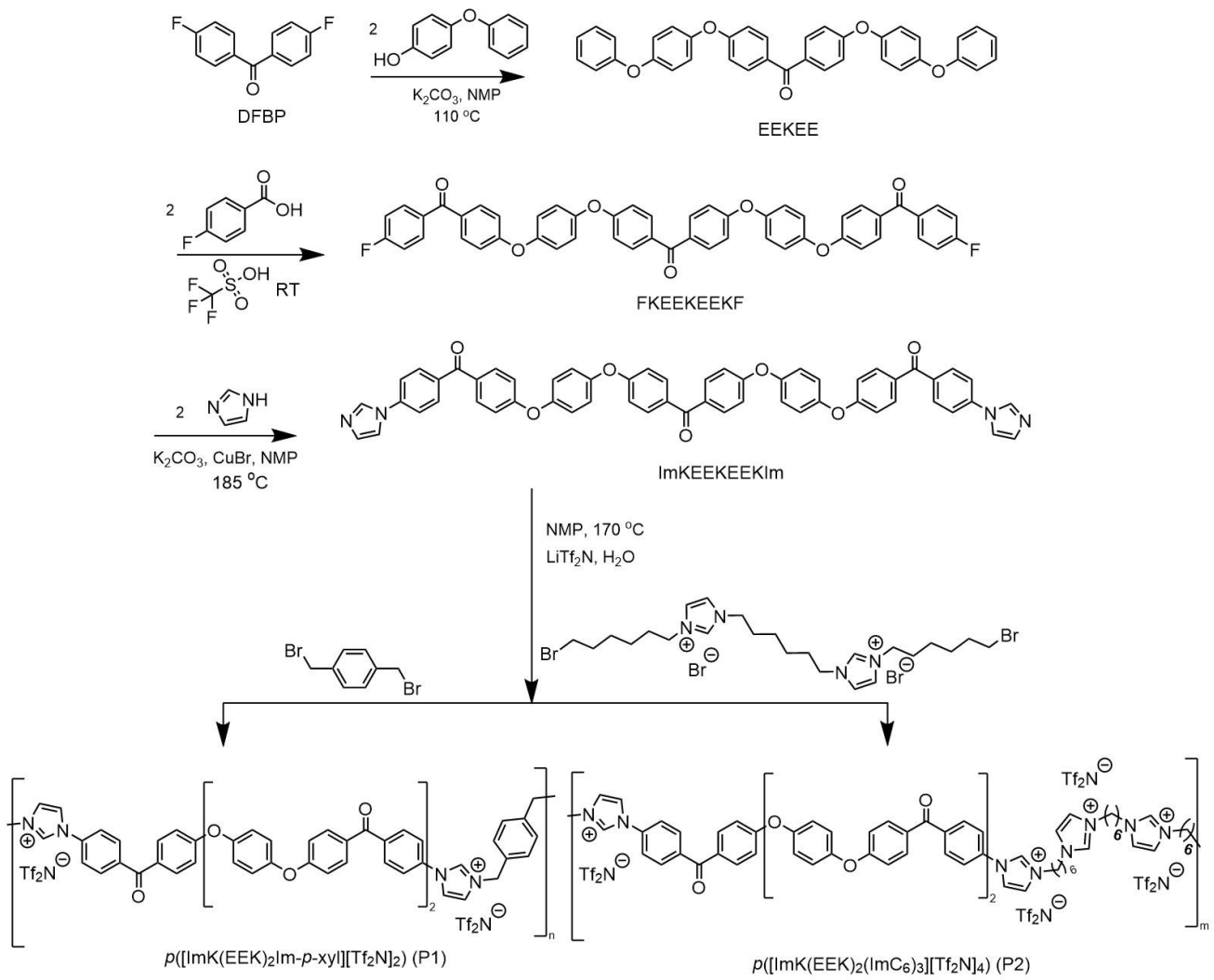

Scheme 1. Synthetic overview of $[Tf_2N]^-$ salts of imidazolium-functionalized poly(ether ether ketone)-ionenes with aromatic and aliphatic linkages.

extensively synthesized and characterized different PEEK oligomers with varied molecular weight.[38] Utilizing the exceptional properties of PEEK polymers and ILs, we designed a strategy to synthesize imidazole-terminated PEEK (Im-PEEK-Im) oligomers to examine the effect of the number of PEEK repeat units on gas separation properties. Simple and straightforward synthetic methods were employed to prepare ($ImK(EEK)_2Im$) monomer which was then polymerized via Menshutkin reaction with two different comonomers (*p*-dibromoxylene and 1,6-((3,3'-di(bromohexyl) bisimidazolium) hexane (2 Br^- salt)) followed by anion-exchange to attain *p*($[ImK(EEK)_2Im$-*p*-$xyl][Tf_2N]_2$) and *p*($[ImK(EEK)_2(ImC_6)_3][Tf_2N]_4$) ionenes, respectively. This is the first example to report the reactive Im-PEEK-Im oligomers and their corresponding polymers, and the successfully application of such materials as gas separation membranes. The PEEK-ionene composites were well characterized by different spectroscopic techniques to understand the structural modification after combining with free IL. Notably, these newly developed PEEK ionenes are of high molecular weight and the IL-impregnated PEEK-ionene matrix has greatly impacted the physical properties as well as the gas separation properties.

EXPERIMENTAL SECTION

Materials.

4,4'-difluorobenzophenone (DFBP, >99%), 4-phenoxyphenol (>95%) were purchased from TCI (Portland, OR, US). Potassium carbonate anhydrous (K_2CO_3, 99%), dimethylacetamide (DMAc, 99.5%), and 1,6-dibromohexane were purchased from BeanTown Chemical (Hudson, NH, USA). Sodium carbonate (Na_2CO_3, 98%) was purchased from Alfa Aesar (Tewksbury, MA, US). Trifluoromethanesulfonic acid and imidazole were purchased form Sigma-Aldrich (Saint-Louis, MO, USA). Lithium bistriflimide ($LiTf_2N$) was purchased from *io-li-tec* (Heilbronn, Germany). 4-Fluorobenzoic acid (99%) was purchased from Chem-Impex international Inc. (Wood Dale, IL, US). Copper (I) bromide (CuBr) was purchased from STREM chemicals (Newburyport, MA, US). α,α'-dibromo-*p*-xylene was purchased from Honeywell Riedel-de Haën AG (Seelze, Germany). Sodium

hydroxide (NaOH) was purchased from Fisher Scientific (Hampton, NH). Dichloromethane (DCM), acetone, acetonitrile (ACN), tetrahydrofuran (THF), diethyl ether (Et_2O), dimethylformamide (DMF), *N*-methyl pyrrolidone (NMP), and dimethylsulfoxide (DMSO) were ACS grade. All chemicals and solvents were used without further purification.

Material Characterization.

Nuclear magnetic resonance (^{1}H and ^{13}C NMR) spectra of the newly synthesized monomers, intermediates, and PEEK-ionene polymers were obtained on a Bruker Avance (500 or Neo500 MHz) instrument using deuterated dimethyl sulfoxide (DMSO-d_6) as a reference. Fourier transform infrared (FT-IR) spectra were recorded using a Perkin Elmer Spectrum 2 ATR-FTIR spectrometer in the range of 400–4000 cm^{-1} at a resolution of 2 cm^{-1}. Thermogravimetric analysis (TGA) of all the samples were conducted using TGA7 thermogravimetric analyzer (Perkin-Elmer Inc., USA) by heating the samples from room temperature (RT) to 700 °C at a heating rate of 10 °C min^{-1} under N_2 flow. The glass transition temperature (T_g) was measured using TA instruments (New Castle, DE, USA) from -40 to 250 °C with a scan rate of 10 C min^{-1} under N_2 flow. The number average molecular weight (M_n) was determined using matrix assisted laser desorption ionization time-of-flight mass spectrometry (MALDI-TOF MS) using a Bruker Rapiflex instrument (Billerica, MA, USA). The PEEK-ionenes were dissolved in DMAc and spotted onto a MALDI plate and allowed to evaporate for 24 h. After drying, 20 µL of 10 mg mL^{-1} dithranol solution and 10 mg mL^{-1} sodium iodide solution was spotted on the polymer. The wide-angle X-ray diffraction (WAXD) patterns were recorded using a Bruker D8 Discover 2θ range was recorded from 5 to 90° with a scan rate of 4° min^{-1} for the polymer samples. The interchain distance (*d*-spacing) values were calculated using Bragg's law ($d = \lambda/2\sin\theta$) and Diffrac-EVA software (Bruker, Billerica, MA, USA). The thickness of membranes was determined using a digital micrometer (Mitutoyo American Co.) and confirmed with scanning electron microscopy (SEM). The cross-section of membranes was captured on a Thermo Scientific Apreo FE-SEM at a magnification between 80× and 250×. The densities of membranes were measured experimentally using a top mount electronic Mettler Toledo balance paired density kit (Product MS-DNY-54). According to Archimedes' principle, each polymer was weighed in air (W_o) and heptane (W_l) and the measurements were performed at ambient temperature in triplicates by the buoyancy method. The density (ρ) was calculated as follows:

$$\rho = w_0 / (w_l - w_0) \times \rho_l$$

Solid-state magic-angle-spinning (MAS) ^{1}H, ^{13}C and ^{19}F NMR of the PEEK-ionene + IL composites were performed on a 600 MHz Bruker Avance III spectrometer using a home-built 5 mm HX probe at a spinning speed of 6 kHz. The probe was equipped with a custom-designed magnetic susceptibility-matched wire for enhanced spectra resolution that is needed to distinguish the semi-liquid component of IL incorporated into the ionenes.[39] The 90° pulse width was 5.0 µs for ^{1}H, 5.5 µs for ^{13}C and 6.0 µs for ^{19}F. For ^{1}H and ^{19}F experiments, *d*1 array was used to make sure that the relaxation delay was long enough for the magnetization to be fully relaxed between each scan for quantitative analysis of the different IL components. The ^{1}H, ^{13}C and ^{19}F NMR MAS spectra were referenced to adamantane and trifluoro acetic acid with ^{1}H at 1.9 ppm, ^{13}C at 29.5 and 38.4 ppm, and ^{19}F at -76.55 ppm, respectively.

Synthesis.

Synthesis of ImK(EEK)$_2$Im oligomer

Synthesis of bis(4-4(-phenoxyphenoxy)phenyl)methanone (EEKEE)

In a 500 mL round bottom flask (rbf), 4,4'-difluorobenzophenone (20.0 g, 92 mmol), 4-phenoxyphenol (32.4 g, 193 mmol), and K_2CO_3 (26.6 g, 193 mmol) were dissolved in 200 mL of NMP under argon (Ar) atmosphere, and the reaction mixture was heated at 185 °C for 24 h. After cooling the flask to room temperature (RT), the reaction mixture poured slowly into vigorously stirred ice cold deionized (DI) water to precipitate the solid product. The precipitate was filtered and dried under vacuum oven at 80 °C for 2d. The obtained solid powder was recrystallized in toluene at reflux temperature for 12 h and filtered to obtain a light tan powder. Yield (49.23 g, 97.5%). ^{1}H NMR (500 MHz, DMSO-d_6) δ 7.77 (d, J = 9.0 Hz, 4H), 7.41 (t, J = 7.5 Hz, 4H), 7.20 (d, J = 8.5 Hz, 4H), 7.15 (t, J = 7.0 Hz, 2H), 7.11 (dd, J = 6.0, 8.5 Hz, 8H), 7.05 (d, J = 8.0 Hz, 4H).

Synthesis of (((((carbonylbis(4,1-phenylene))bis(oxy))bis(4,1-phenylene))bis(4,1-bisphenylene))bis(4-fluorophenyl)methanone, FK(EEK)$_2$F.

The synthesis of FK(EEK)$_2$F has already been described elsewhere.[38] In a 500 mL rbf, 110 mL (185.8 g, 1248 mmol) of trifluoromethanesulfonic acid was added to EEKEE (9.6 g, 17 mmol) and the reaction flask was cooled to 0 °C for 30 min. Then 4-fluorobenzoic acid (5.4 g, 38 mmol) was added slowly for 30 min at 0 °C and then stirred at RT for 24 h. The solution was slowly poured in 1.0 L of aq. Na_2CO_3 (1.2 M) to precipitate the product. The solid material was filtered, washed multiple times with hot DI water and hot acetone and then refluxed for 24 h in water and acetone, respectively. The solids were collected by filtration and dried under vacuum at RT for 24 h. The obtained solid was recrystallized twice from NMP to give an off-white powder. Yield (12.5 g, 90%). ^{13}C NMR (125 MHz, methanesulfonic acid) δ 201.33, 199.46, 177.58, 169.59, 168.30, 168.22, 151.20, 150.77, 140.30, 139.15, 138.24, 138.15, 140.30, 139.15, 138.24, 138.15, 126.62, 123.72, 123.47, 123.09, 118.06, 117.86, 117.59, 117.41.

Synthesis of (((((carbonylbis(4,1-phenylene))bis(oxy))bis(4,1-phenylene))bis(4,1-bisphenylene))bis(4-(1H-imidazol-1-yl))methanone, ImK(EEK)$_2$Im.

Into a 250 mL rbf, a mixture of FK(EEK)$_2$F (10 g, 16 mmol), imidazole (2.57 g, 38 mmol), K_2CO_3 (6.08 g, 44 mmol), and CuBr (0.36 g, 3 mmol) were added under Ar atmosphere. NMP (100

mL) was added to the flask and equipped with a reflux condenser, and the reaction mixture was heated at 185 °C for 24 h. After this time, the reaction mixture was cooled to RT and the solid product was precipitated in DI water and ice. The solid was filtered and washed with copious amounts of DI water and then dried in a vacuum oven at 100 °C to obtain a dark solid product. Yield 10.5 g, 95%). ^{1}H NMR (500 MHz, DMSO-d_6) δ 9.53 (bs, 2H), 8.47 (bs, 2H), 8.07−7.64 (bs, 19H), 7.35−5.98 (m, 15H).

Comonomer synthesis [(C_6BrIm)$_2C_6$][Br]$_2$

Synthesis of 1,6-di(1*H*-imidazol-1-yl)hexane

The synthesis of sodium imidazolate was performed in a manner similar to our earlier work.[40] The pale-yellow product was cooled and stored in the dark glass container. Yield (34.08 g, 84.8 %). A mixture of sodium imidazolate (4.84 g, 58 mmol) and 1,6-dibromohexane (5.90 g, 24 mmol) were dissolved in 30 mL of THF, and the reaction mixture was stirred at 65 °C for 24 h. After cooling the flask, the reaction mixture was filtered, and the organic solvent was concentrated on a rotary evaporator. The obtained solid material was dissolved in DCM to remove any additional precipitates and the process was repeated twice. The filtered solution was concentrated on a rotary evaporator, and finally dried under vacuum at 60 °C to attain solid product. Yield (3.78 g, 72%). ^{1}H NMR (500 MHz, DMSO-d_6) δ 7.60 (s, 2H), 7.14 (s, 2H), 6.87 (s, 2H), 3.91 (t, J = 7.0 Hz, 4H), 1.72−1.61 (m, 4H), 1.25−1.16 (m, 4H).

Synthesis of 1,1'-(hexane-1,6-diyl)bis(3-(6-bromohexyl)-1*H*-imidazol-3-ium dibromide, ([(C_6BrIm)$_2C_6$][Br]$_2$)

A mixture of 1,6-di(1*H*-imidazol-1-yl)hexane (3.78 g, 17 mmol) and a large excess amount of 1,6-dibromohexane were taken in 80 mL of ACN and heated at reflux for 24 h. During the reaction, two separate phases were noticed. After cooling the flask to RT, the organic layer was decanted, and the viscous material was washed with diethyl ether (3 × 50 mL) to remove unreacted starting materials. Finally, the solid product was concentrated on a rotary evaporator followed by vacuum drying at 60 °C overnight. Yield (10.98 g, 90%). ^{1}H NMR (500 MHz, DMSO-d_6) δ 9.35 (d, J = 4.5 Hz, 2H), 7.84 (d, J = 2.5 Hz, 4H), 4.18 (t, J = 7.0 Hz, 8H), 3.53 (t, J = 6.5 Hz, 4H), 1.86−1.74 (m, 12H), 1.33−1.21 (m, 12H).

Polymer synthesis.

Synthesis of *p*[ImK(EEK)$_2$Im-*p*-xyl][Tf_2N]$_2$ (P1)

In a 250 mL heavy walled glass pressure flask, a mixture of ImK(EEK)$_2$Im (2.20 g, 3.21 mmol) and 1,4-α,α'-dibromo-*p*-xylene (0.85 g, 3.21 mmol) were added to 30 mL of NMP. The flask was sealed properly with a PTFE cap and DuPont Kalrez O-ring and heated at 170 °C for 48 h. After cooling the flask to RT, the reaction mixture was poured into a vigorously stirred $LiTf_2N$ (2.30 g, 8.03 mmol) in 30 mL of DI water and then stirred at 100 °C for 1 h. The precipitate was filtered and washed with hot DI water and then dried under vacuum oven at 100 °C for 48 h to yield a dark solid product. Two step yield (3.86 g, 90%). ^{1}H NMR (500 MHz, DMSO-d_6) δ 10.13 (s, 2H), 8.47 (s, 2H), 8.22−6.81 (m, 34H), 5.56 (s, 4H).

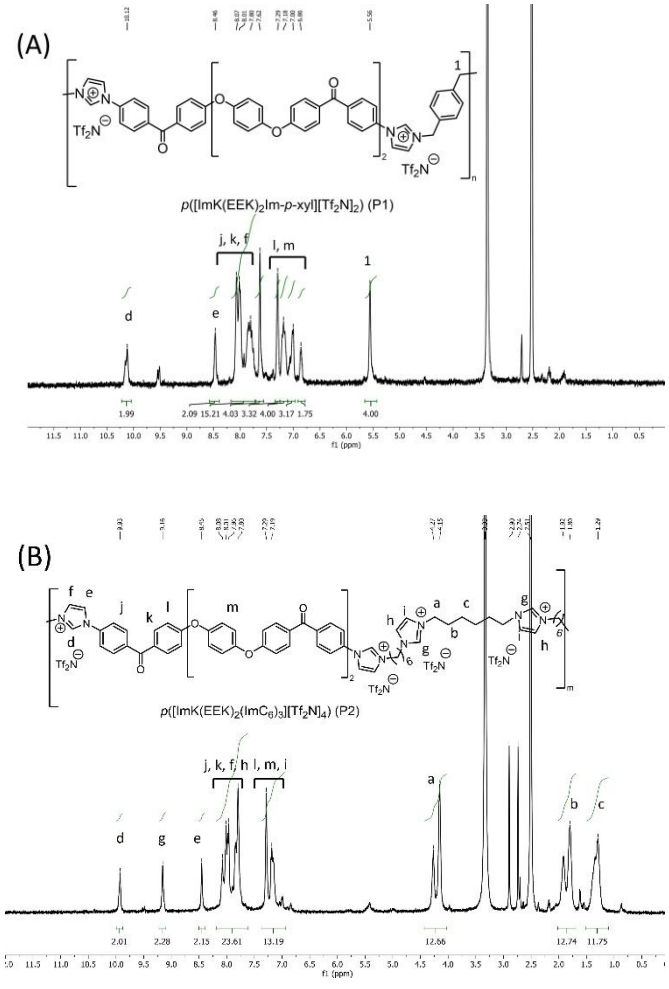

Figure 1. ^{1}H-NMR of the (A) *p*([ImK(EEK)$_2$(ImC$_6$)$_3$][Tf_2N]$_4$ (P1), and (B) *p*([ImK(EEK)$_2$Im-*p*-xyl][Tf_2N]$_2$ (P2) ionenes.

Synthesis of *p*[ImK(EEK)$_2$(ImC$_6$)$_3$][Tf_2N]$_4$ (P2)

The polymer *p*[ImK(EEK)$_2$(ImC$_6$)$_3$][Tf_2N]$_4$ was synthesized by the same method as above *p*[ImK(EEK)$_2$Im-*p*-xyl][Tf_2N]$_2$. In brief, the mixture of ImK(EEK)$_2$Im (3.0 g, 3 mmol) and [(C_6BrIm)$_2C_6$][Br]$_2$ (2.4 g, 3 mmol) in 30 mL of NMP and heated to 170 °C for 48 h under Ar atmosphere. A dark solid product was obtained after two steps, yield (6.9 g, 85%). ^{1}H NMR (500 MHz, DMSO-d_6) δ 9.93 (s, 2H), 9.16 (s, 2H), 8.45 (s, 2H), 8.25−7.56 (m, 24H), 7.41−6.94 (m, 14H), 4.34−4.22 (m, 4H), 4.22−4.07 (m, 8H), 2.06−1.66 (m, 12H), 1.51−1.16 (m, 12H).

Synthesis of 1-butyl-3-methyl-1H-imidazol-3-ium bistriflimide [C_4mIm][Tf_2N]

The title product was synthesized in our lab on large scale and a detailed synthesis was reported in our previous work.[41] Figure S21 shows the corresponding ^{1}H-NMR spectra.

Membrane preparation

All the membranes were prepared by solution-casting methods. The PEEK-ionene polymers were dissolved in DMAc (1:9 w/w) and a stoichiometric equivalent amount of "free" [C_4mIm][Tf_2N] IL was added to obtain neat and composite membranes, respectively. The solution was stirred at RT or 50 °C for overnight and filtered through a glass pipette with glass wool to remove any insoluble materials. The solution was slowly casted onto a clean Teflon support followed by slow evaporation of solvent under vacuum oven at 40 °C for 48 h and then slowly raised to 100 °C for over a period of 72 h. After cooling to RT, the membranes can be easily peeled off the Teflon support and stored at RT for analysis.

Gas permeation measurements

The pure gas permeation experiments of PEEK-ionene + IL composite membranes were performed using high-vacuum time lag apparatus based on the conventional constant volume/variable pressure method. The membranes were "masked" on both sides using an adhesive aluminium tape to confine gas permeation through a fixed membrane area of 1⁄2 in diameter (A = 0.7125 cm^2) known as the aluminium "tabbing'' method. Before the gas permeation measurements, the units (feed and permeate) are held under vacuum (< 0.01 psia) for 24 h. All the single gas permeation measurement were conducted at 20 °C and the feed pressure was ~2 atm (~30 psia) against initial downstream vacuum (<0.01 psia). The pressure rise versus time and temperature were monitored and recorded using the latest version of LabView software (National Instruments, Austin, TX, USA). The gas permeability of each membrane was determined from the from the linear slope of the plot of downstream pressure rise versus time plot (dp/dt) according to the following equation:

$$P = (273/76) \times (\mathrm{V}\, l/ATP_O) \times (dP/dt)$$

where *P* is the permeability expressed in Barrer (1 Barrer = 10^{-10} cm^3 (STP) cm cm^{-2} s^{-1} $cmHg^{-1}$); V (cm^3) is the downstream volume; l (cm) is the thickness of the membrane; A (cm^2) is the effective gas permeation area of the membrane; T(K) is the measurement temperature; P_0 (Torr) is the pressure of the feed gas at the upstream; and dp/dt is the rate of permeate absolute pressure for steady state. The ideal permselectivity ($\alpha_{A/B}$) for a give gas pair (A and B) was calculated from the ratio of the individual gas permeability coefficients as, P_A/P_B.

Results and discussion

Structural Characterization

Scheme 1 shows a simple and straightforward three-step synthetic route for the preparation of an imidazole-functionalized PEEK oligomer [ImK(EEK)$_2$Im]. The first two-step was adopted from previously reported work with slight modification.[38] Firstly, nucleophilic aromatic substitution reaction of DFBP with a slight excess of 4-phenoxyphenol was performed in the presence of K_2CO_3 in NMP under Ar atmosphere to give EEKEE as an off-white powder. The second step was followed by Friedel-Crafts acylation in presence of trifluoromethanesulfonic acid acts as both solvent and catalyst. Both intermediates were characterized using NMR spectroscopy (^{1}H and ^{13}C) and shown in Figures S1–S2. Notably, the intermediate building block FK(EEK)$_2$F is soluble in high-boiling polar aprotic solvents such as NMP on heating or methanesulfonic acid ($MeSO_3H$) at RT. The ^{13}C-NMR was performed in $MeSO_3H$ at RT and the signals agree well with the chemical structure and matches with the published report.[38] Finally, the imidazole group was substituted using Ullmann coupling to achieve an imidazole-functionalized PEEK oligomer (ImK(EEK)$_2$Im), see Figure S3 for NMR spectra. This newly developed monomer is soluble in polar aprotic solvents such as NMP, DMAc, and DMSO at elevated temperatures but precipitates immediately after cooling due to its high tendency to crystallize. In the past, the integration of different functional groups into the PEEK main chain through pre- or post-modifications were usually achieved to improve the performance and efficiency of the materials.[17, 21] However, the ImK(EEK)$_2$Im synthesized in this study was not reported earlier in the literature. By employing this approach, we can prepare different PEEK oligomers and simultaneously utilize the modularity of imidazole as a building block to develop distinct functional moieties for a wide variety of applications.

Two new imidazolium-functionalized PEEK-ionenes with bistriflimide ([Tf_2N]) anions were prepared via Menshutkin reaction between the ImK(EEK)$_2$Im monomer and dibromo-xylene (aromatic linker) or dibromohexyl containing-bis(imidazolium)hexane dibromide salt (aliphatic linker), respectively in NMP at 170 °C for 48 h, followed by anion-exchange with LiTf_2N. The synthesis and corresponding NMR spectra for the aliphatic comonomer were shown in Figures S4–S6. Figure 1 displays the ^{1}H-NMR spectra for the PEEK-ionenes, *p*([ImK(EEK)$_2$Im-*p*-xyl][Tf_2N]$_2$) and *p*([ImK(EEK)$_2$(ImC_6)$_3$][Tf_2N]$_4$) and the proton signals are well assigned with their chemical structures. Typically, the formation of imidazolium cation increases the acidity of the protons resulting in a shift in proton signals towards downward spectra. The characteristic peaks of the imidazolium protons next to aromatic and aliphatic linkages at 10.33–8.43 ppm in PEEK-ionenes, confirmation the formation of the imidazolium cation, and indicative of successful condensation polymerization. At the same time, the proton signal of the benzylic group at 5.56 ppm in *p*([ImK(EEK)$_2$Im-*p*-xyl][Tf_2N]$_2$) and the proton signal of methylene groups at 4.21, 1.86, and 1.29 ppm in *p*([ImK(EEK)$_2$(ImC_6)$_3$][Tf_2N]$_4$), further confirmed the formation of PEEK-ionenes. Here onwards *p*([ImK(EEK)$_2$Im-*p*-xyl][Tf_2N]$_2$) and *p*([ImK(EEK)$_2$(ImC_6)$_3$][Tf_2N]$_4$) ionenes are denoted as P1 and P2, respectively.

Additionally, the chemical structures of intermediates and PEEK-ionenes were verified by FT-IR analysis, displayed in Figure 2. The peak around 1645 cm^{-1} corresponds to the stretching vibration of the ketonic C=O bond, while the peak around 1586 cm^{-1} and 1498 cm^{-1} corresponds to the stretching vibration of the aromatic C=C bonds. Further, the strong peak around 760 cm^{-1}, and 1242 and 1300 cm^{-1} correspond to the stretching vibration of the aromatic fluorine and aryl ether (Ar–O–Ar), respectively. While the peak around 930 cm^{-1} corresponds to

the asymmetric stretching vibration of aryl ketone (Ar–(C=O)–Ar). The peaks around 1040, 1348, 1378, and 1570 cm^{-1} correspond to the in-plane symmetric and asymmetric vibration peaks of characteristic imidazole and imidazolium ring obtained after Ullmann coupling and Menshutkin reactions, respectively. Furthermore, the strong peaks around 1050 (SNS), 1190, 1225 (CF_3), and 1348 (SO_2) cm^{-1} correspond to the presence of Tf_2N anion introduced through anionic exchange. At last, the peaks around 3153 cm^{-1}, and 2940 cm^{-1} correspond to the stretching vibration of aromatic and aliphatic C–H bond, respectively, while the peaks around 1330, 1435, and 1220 cm^{-1} correspond

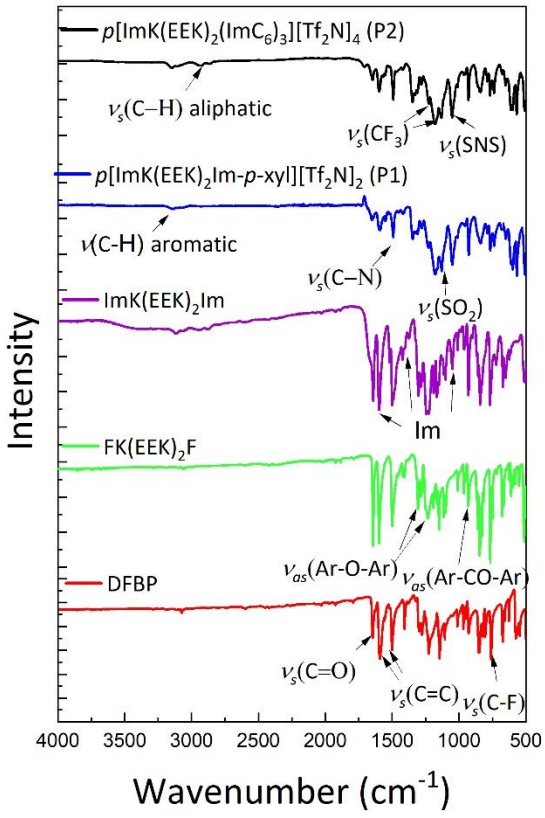

Figure 2. FT-IR spectra of intermediates and neat PEEK-ionene polymers synthesized in this study.

to CH_2 bending of aliphatic carbons. It is worth noting that the intensity of the C=O band decreased after anion exchange and little-to-no change in FT-IR spectra was observed after the incorporation of free IL. Overall, the FT-IR peaks were assigned and matches well with the structures indicating the successful synthesis of monomer and polymeric PEEK ionenes.

Further, these two PEEK-ionenes exhibit high molecular weights (including both cation and anion), determined by the MALDI-TOF MS techniques (Figures S7–8). The P1 and P2 ionenes had molecular weight of M_n ~79 KDa and ~99 KDa, respectively. The degree of polymerization (DP) and repeat units (X_n) for PEEK ionenes can be determined using Carothers' equation. The DP and X_n values for P1 and P2 ionenes are ~0.980 and ~0.973, and ~51 and ~37, respectively. The decrease in the calculated X_n units for the latter ionene might be attributed to many factors including, anion weight fraction in the polymer, comonomer connectivity, the ability of ionized molecules to fly, and charge density.

Membrane formation

When compared to the pristine PEEK polymer and intermediates synthesized in the study, both the newly developed PEEK-ionenes displayed improved solubility in DMF, DMSO, DMAc, and NMP at 50 °C. Although, the PEEK-ionenes are soluble in common organic solvents but required heating to fully dissolve. The presence of aliphatic and aromatic comonomer groups in PEEK-ionene disrupted the regularity of polymer chains and enhanced the solubility. Hence, the solubility of the newly synthesized PEEK-ionenes allows for the formation of thin films for the gas separation studies. The membranes were prepared by solution casting methods using DMAc as a solvent. Figure 3 shows photographs of the PEEK-ionenes and composites prepared in this study. Unfortunately, the neat PEEK-ionenes are very brittle (Figures 3A, E), possibly due to the rigidity of aromatic polymer backbone. Incorporation of 1 eq. of free IL into the neat PEEK-ionenes resulted in mechanically stable, free-standing membranes. As the addition of free IL increased, the flexibility of the membranes greatly increased. It must be noted that neat (i.e., commercial) PEEK would have no ability to hold an IL within its structure, whereas the newly developed PEEK ionenes can easily retain IL within their structures due to coulombic interactions between the ions in the backbone and free IL, a macroscopic indication of the molecular-level structures of the PEEK ionene.

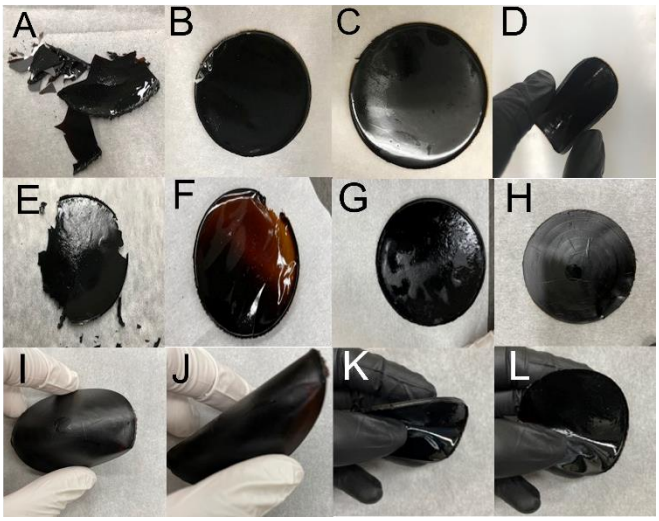

Figure 3. Photographs of PEEK-ionenes with varied comonomer connectivity and their corresponding composites. (A) *p*([ImK(EEK)$_2$Im-*p*-xyl][Tf_2N]$_2$ (P1) (B) P1 + 1 eq. [C_4mIm][Tf_2N] IL, (C, D) P1 + 2 eq. IL, (E) *p*([ImK(EEK)$_2$(ImC_6)$_3$][Tf_2N]$_4$ (P2), (F) P2 + 1 eq. IL, (G, I, J) P2 + 2 eq. IL, and (H, K, L) (F) P2 + 3 eq. IL composite. Photos D, I, J, K, L displays the flexibility of their respective PEEK-ionene composites.

Figure 3D displays the flexibility of the PEEK-ionene composite for P1 + 2 eq. IL. Similarly, Figure 3I–J and Figure 3K–L shows the flexibility of the PEEK-ionene composites for P2 + 2 eq. IL and P2 + 3 eq. IL, respectively. Importantly, no sign of IL discharge was observed from these composite membranes.

Nevertheless, presence of free IL in the PEEK-ionene polymer yields homogenous and flexible membranes plausibly due to strong molecular interactions between the imidazolium-functionalized PEEK-ionenes and free IL. These intermolecular interactions will exclusively occur in the ionic segment of the PEEK ionene and are likely the main contributor to enhancing gas diffusivity. Further, the cross-sections of these membranes are in the range of 177–255 µm (Figures S9–13). The difference in thickness is mainly due to the PEEK-ionene concentrations, IL amounts, and area exposed for gas separation. The SEM analysis shows that PEEK-ionene + IL composites are dense and non-porous membranes without any defects or cracks.

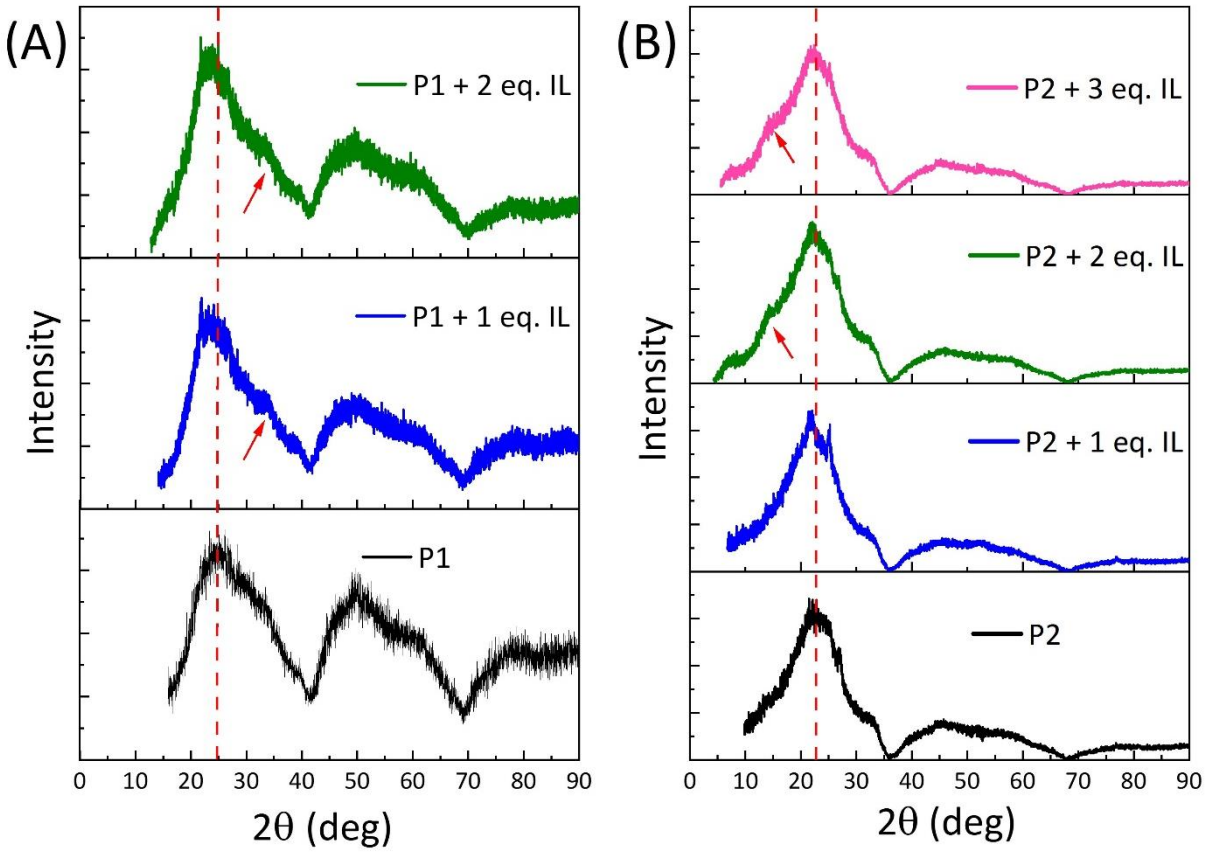

Figure 4. Wide-angle X-ray diffraction patterns for PEEK-ionene polymers and its corresponding composites. (A) *p*([ImK(EEK)$_2$Im-*p*-xyl][Tf$_2$N]$_2$ (P1) (B) *p*([ImK(EEK)$_2$(ImC$_6$)$_3$][Tf$_2$N]$_4$ (P2). The red arrows show the rise of extra peaks after addition of free [C$_4$mIm][Tf$_2$N] IL into PEEK-ionenes

Wide angle X-ray diffraction

To further understand the structural effects of connectivity (aromatic and aliphatic) and the free IL loading in the main-chain polymer, wide-angle X-ray diffraction (WAXD) was investigated on newly developed PEEK-ionene and composite membranes. As displayed in Figure 4, the absence of sharp diffraction peaks from the bulk samples and their corresponding composites indicates the amorphous nature of the polymers. A similar amorphous XRD profile pattern was observed for "pristine" PEEK polymers by Thankamony *et al.*,[33] which are in good agreement with our newly developed neat PEEK-ionenes. In detail, the aliphatic containing bulk PEEK-ionenes displayed single-peak distribution peaks around 16–42° (2θ), and broader and less intense peaks at higher angles. Whereas the xylyl containing bulk PEEK-ionenes exhibited bimodal distribution patterns around 16–42° and 42–70° (2θ). This suggests that comonomer linkages in these imidazolium PEEK-ionenes played a significant role in chain packing architecture. This can be further corroborated by the intersegmental (*d*) spacing from the diffraction patterns of PEEK-ionenes. The *d*-spacing values were calculated from the main halo peak, which was occurred between 2θ = 21–27° for neat P1 and P2 ionenes are 4.14 Å (2θ = ~24.97°) and 4.45 Å (2θ = ~23.17°), respectively. This difference in *d*-spacing are mainly attributed to the structural features of linker groups in the PEEK-ionene polymers, thus influence the free volume and gas transport properties.

Further, the incorporation of free IL into the polymer network usually results in the broadening of peaks in the XRD spectrum. When 1 eq. of free IL was added to a neat PEEK-ionene polymer, a bimodal distribution peak and a single distribution peak was observed for aromatic and aliphatic linkages, respectively. In detail, for P1+ 1 eq. IL composite, the primary and secondary peaks were centred around 23.6° and 33.8° (2θ) with *d*-spacings of 4.38 Å and 3.07 Å, respectively. Similarly, the primary peaks were centred around 22.1° (2θ) with a *d*-spacing of 4.67 Å for P2 + 1 eq. IL composite. Overall, the regularity of the polymeric membrane was greatly affected

with respect to the comonomer linkages. The *d*-spacing for PEEK-ionene composites has slightly improved irrespective of the nature of the comonomer connectivity, where the free IL occupies the voids spaces in the neat PEEK ionenes and loosen the chain packing network. Surprisingly, further addition of IL resulted a bimodal distribution peak for P2 + 2 eq. IL or 3 eq. IL. A new peak appeared at a lower angle of the primary peak as opposed to the P1 + 1 eq. IL ionene composite. This confirms that the comonomer linkages exhibit distinct polymeric architecture, macromolecular interactions, and free IL effects on the ordering patterns of the PEEK-ionene polymer. The entire *d*-spacing of PEEK-ionenes were depicted in Table 1. These XRD profiles show the effect of IL on the polymer matrix, but it is worth noting that there is little to-no-change in the *d*-spacing even after increasing the amount of IL content. We assume that the aromatic and aliphatic segments generate irregularities in the PEEK-ionene polymer chain, and the initial amount of free IL effectively opens the gaps in the polymer matrix. Further addition of IL associates with ionic imidazolium segments in the main-chain polymer.[42] Based on the nature of the comonomer connectivity, the amount of free ILs occupied within the ionene-matrix varied substantially and the extra peaks might influence the gas properties, especially gases such as CO_2 (3.3 Å) and CH_4 (3.8 Å), which have different kinetic diameters.

Table 1. Physical and thermal properties of PEEK ionene-IL composite membranes

Polymer	Notation	*d*-spacing (Å)	Density[a] g cm^{-3}	Thermal stability[b] T_{dcp} (°C)
p([ImK(EEK)$_2$Im-*p*-xyl][Tf$_2$N]$_2$	P1	4.14	1.49	363.4
p([ImK(EEK)$_2$Im-*p*-xyl][Tf$_2$N]$_2$ + 1 eq. IL	P1 + 1 eq. IL	3.07, 4.38	1.50	375.9
p([ImK(EEK)$_2$Im-*p*-xyl][Tf$_2$N]$_2$ + 2 eq. IL	P1 + 2 eq. IL	3.08, 4.38	1.51	389.5
p([ImK(EEK)$_2$(ImC$_6$)$_3$][Tf$_2$N]$_4$	P2	4.45	1.46	396.3
p([ImK(EEK)$_2$(ImC$_6$)$_3$][Tf$_2$N]$_4$ + 1 eq. IL	P2 + 1 eq. IL	4.67	1.49	378.5
p([ImK(EEK)$_2$(ImC$_6$)$_3$][Tf$_2$N]$_4$ + 2 eq. IL	P2 + 2 eq. IL	4.67, 7.14	1.49	389.5
p([ImK(EEK)$_2$(ImC$_6$)$_3$][Tf$_2$N]$_4$ + 3 eq. IL	P2 + 3 eq. IL	4.66, 7.26	1.46	383.1

[a]The samples were measured in triplicates with standard deviation of 0–2%. [b]The decomposition temperature T_{dcp} denotes the thermal onset of decomposition, signifying the 10% total mass loss during TGA scanning at 10 °C min^{-1} under N_2 flow.

Table 1 shows the density of the newly developed neat PEEK-ionenes and PEEK-ionene + IL composites. The density of aliphatic and aromatic comonomers in imidazolium-functionalized PEEK-ionenes polymers shows no significant decrease with the addition of 1 eq. IL into the neat PEEK-ionene polymers. The results further validate that as the *d*-spacing value increases for PEEK-ionene + 1 eq. IL composites, the density value decreases due to large access to the volume spaces, which are fairly in agreement with the previously published data.[10, 36] However, the further addition of IL content into the membrane has no significant effect on the density values, which matches with the XRD data. Therefore, a considerable modification in the structural orientation of PEEK-ionene and corresponding composites was observed, which impacts the performance of gas transport properties, especially the diffusivity and permeability of the membranes.

Thermal properties

The thermal stabilities of the intermediates (FK(EEK)$_2$F and ImK(EEK)$_2$Im), newly developed PEEK-ionene polymers, and corresponding composite membranes were investigated by thermogravimetric analysis (TGA) under N_2 atmosphere. Table 1 and Figures 5, S14 and S15 depicted the respective TGA profiles. The mass loss of the intermediate FK(EEK)$_2$F oligomer did not occur until about 488 °C (T_{dcp}), indicating a random cleavage of the aryl ether and ketone bonds. A similar TGA

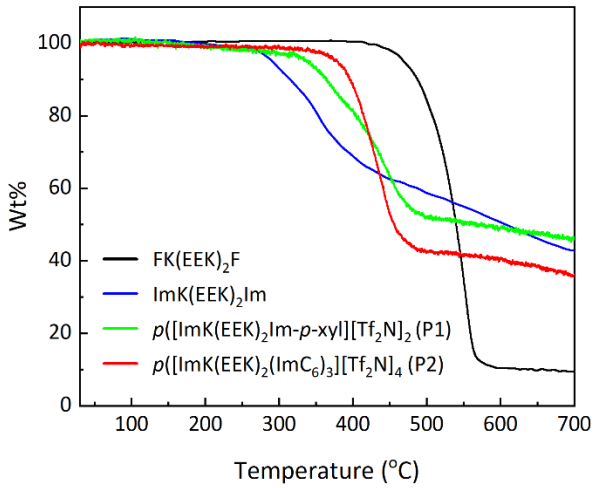

Figure 5. TGA profiles for intermediates ($FK(EEK)_2F$, $ImK(EEK)_2Im$) and PEEK-ionene polymers.

profile was observed for the conventional PEEK polymer.[43, 44] The incorporation of imidazole moiety at both ends, $ImK(EEK)_2Im$ oligomer reduces the thermal stability due to the scission of imidazole that begins at ~260 °C (T_{dcp} = 365.1 °C). But about 50 wt% of carbonaceous char remained at 700 °C when compared to $FK(EEK)_2F$ oligomer (10 wt%), which might provide additional stability to the monomer after first pyrolysis step for different applications. This kind of behaviour was observed to

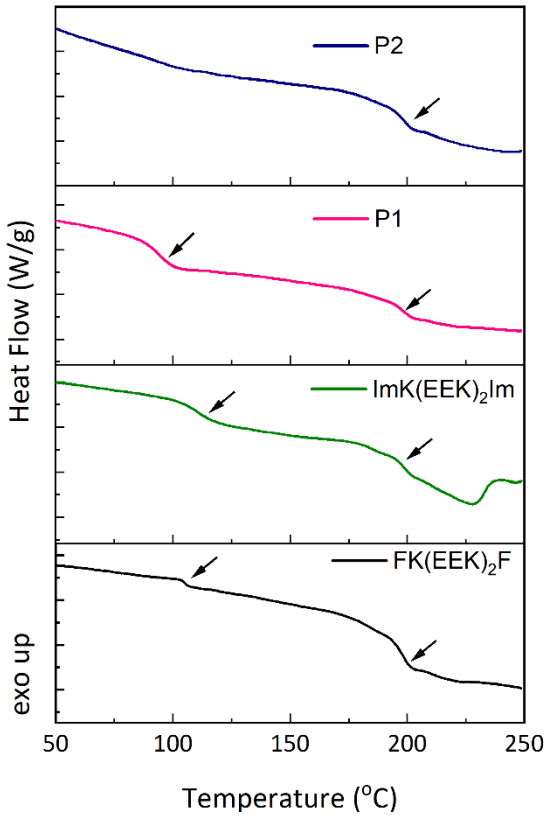

Figure 6. DSC curve of intermediates ($FK(EEK)_2F$ and $ImK(EEK)_2Im$) and PEEK ionene polymers. The transition at ~198 °C is due to the aluminium sample pan.

modified-PEEK polymers.[44] Further, the P1 ionene exhibited two degradations. The first degradation occurred between 325 and 405 °C (T_{dcp} = 363 °C), which was attributed to the decomposition of the xylyl linkage, and the second degradation was attributed to the decomposition of the imidazolium-functionalized PEEK segment. In contrast, a single decomposition temperature around 396 °C was observed for the P2 ionene, and the enhanced stability was attributed to the presence of additional ionic charge moieties in the macromolecular structure. Remarkably, no notable change in the decomposition temperature was observed for membrane composites (Figures S14–15) with the IL loading. This suggests that the free IL in the PEEK-ionene demonstrating strong molecular interactions with the polymer network. Overall, the TGA thermograms exhibited high thermal stability for the PEEK-ionenes that are suitable for gas separation applications, particularly for CO_2 separation process in flue gas streams.[45, 46]

Figures 6 and S16–17 illustrates the thermal transition properties of all intermediates, ionenes, and composites were analyzed by DSC measurements. It is a well-known fact that the chain rigidity and the interchain interactions greatly influence the T_g of the polymer. It worth noting that a transition at around 198 °C was seen for all the samples, is strictly due to the aluminium sample pan used in these measurements. This transition behaviour was observed for other polymers which was reported by Ravula *et al.*[41] The intermediate $FK(EEK)_2F$ exhibited T_g around 105 °C and melting point (T_m) around 225 °C, which is in-line with the robust and semi-crystalline PEEK polymer that exhibited T_g at around ~145 °C.[10] Further, a higher T_g value around 111 °C was observed for the monomer $ImK(EEK)_2Im$ indicates that a slight modification with imidazole moieties lead to increase in T_g value and T_m was observed around ~228 °C. Upon polymerization, the T_g of P1 is 11–16 °C less than that of monomers indicating that charged moiety slightly reduces the rigidity induced by the PEEK segments. In case of P2 ionene and composite polymers, no T_g values were observed even at –40 °C. The integration of IL not only increases the chain mobility of the resultant composites, thus enhancing the gas transport properties of the membranes is expected. Similar finding were observed for the composite polymers after the addition of IL.[47] The detailed explanation on the permeability and diffusion coefficient will be discussed in following sections.

Solid-state magic angle spinning (MAS) NMR

MAS-NMR measurements were performed to further investigate the structural and dynamic changes introduced by incorporating free IL into P1 and P2 membranes. Polymer backbone proton signals are usually too broad and provide little structural information, with only the spinning side bands discernible at 22 – 14 ppm and 0 – -6 ppm (Figure 7A). The relatively sharp proton signals between 0 – 10 ppm belong to free ILs that are incorporated within the neat PEEK-ionene polymers, exhibiting lower mobility than free neat ILs, but much higher mobility than the backbone molecules. Similarly, because ^{13}C NMR signals from polymer backbones are also

ARTICLE

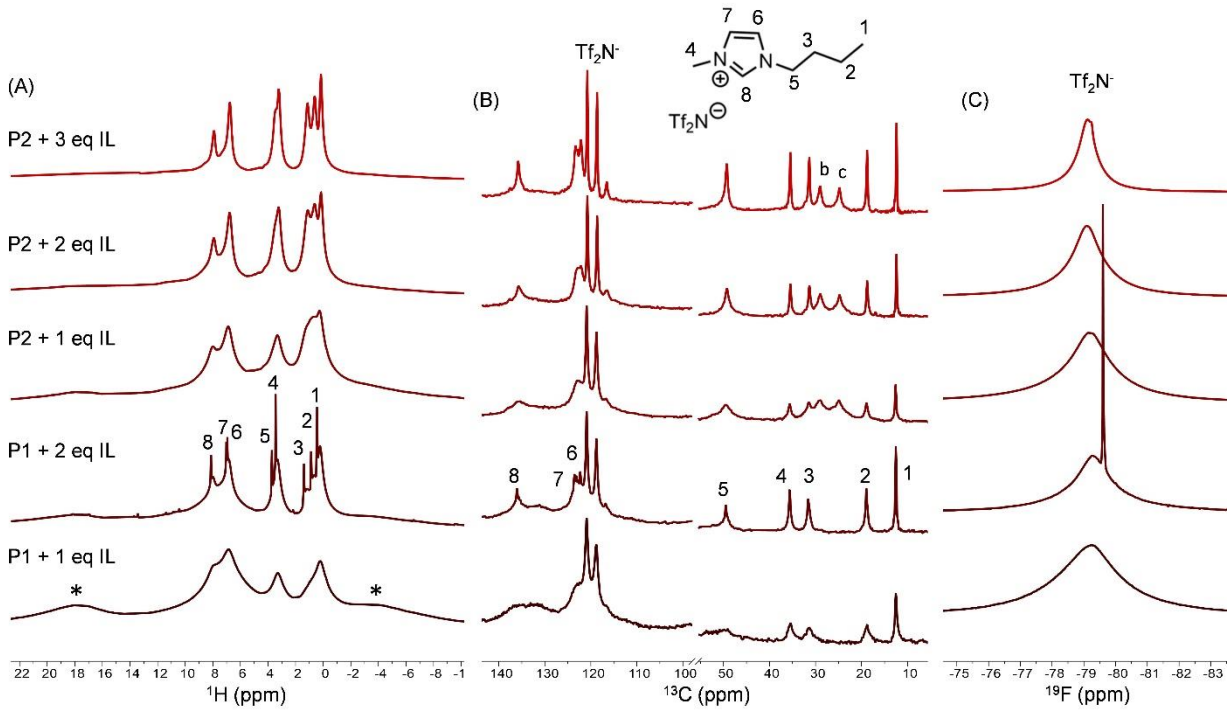

Figure 7. Solid-state MAS NMR of (A) ^{1}H, (B) ^{13}C with ^{1}H decoupling, and (C) ^{19}F of PEEK-ionene + IL composite membranes at a spinning speed of 6 kHz.

broad with relatively long spin-lattice relaxation time constants, direct polarization ^{13}C NMR spectra with a short relaxation delay primarily report signals from ILs (Figure 7B). The ^{19}F NMR spectra report on the terminal CF_3 of Tf_2N^- from both free ILs and polymer counter anions (Figure 7C). By increasing the amount of IL from 1 eq. to 2 eq. in P1, two distinct sets of IL proton signals are observed. Spectral deconvolution (Figure S18) reveals that the broader signals contribute to 90% of total signals and can be assigned as ILs that interact closely with polymer backbone, while the 10% sharper signals arise from loosely bound ILs with higher mobility that may be located at the centre of the IL-rich domains and experience reduced interaction with the polymer chains. The sharper component is also manifested in ^{19}F NMR (Figure S19A), where three components can be attributed to Tf_2N^- that are tightly associated with polymer imidazole rings (the broadest signal), Tf_2N^- that are incorporated in the ionic domains (the broad signal) and the Tf_2N^- from free ILs that experience least confinement effect from the polymer backbones (the sharp signal). The general trend is the same for P2, the ^{1}H, ^{13}C and ^{19}F resonances all become sharper with more incorporated IL, suggesting higher IL mobility at a higher load. Additionally, the ^{13}C signals from alkyl linkers (carbon b and c in Figure 7A) become sharper with increasing IL loading. This can be explained by that the incorporated ILs are in close contact with the IL sections of the polymers, therefore more incorporated ILs lead to larger ionic domains, which in return improve the mobility of polymer molecules in the IL sections. On the other hand, comparing between P1 + 1 eq. IL and P2 + 1 eq. IL, the latter has sharper signals, indicating that higher IL mobility can be achieved with larger IL sections in the polymer. In contrast, comparing the two polymers with 2 eq. IL, the latter has broader signals, implying that more ILs are needed to cover the interactions with the polymer that have larger IL segments. Indeed, we observe a small fraction of highly mobilized IL (similar to free IL) at 3 eq. IL with P2 (Figure S19B). In addition, although the proton signals of polymer backbones are mainly buried in the baseline of ^{1}H NMR spectrum, signal intensities of the spinning sidebands decrease with IL loading (Figure S20), implying that more incorporated ILs lead to more flexible polymer chains. Overall, NMR observations are consistent with the hypotheses (1) ionic domains are formed from the IL sections of the polymers, with the formation of larger ionic domains from larger IL sections; (2) incorporated ILs are primarily located in the ionic domains and interact with IL

sections of the polymers; (3) a high IL loading can produce highly mobilized ILs that may connect ionic domains to form 3D interconnected channels for high CO_2 permeability.

Gas transport properties

The gas transport properties of dense polymeric membranes are of great importance in understanding the separation of greenhouse gas emissions and improving their energy efficiency attributes and recycling processes. To the best of our knowledge, this is the first report to publish on the newly developed precisely segmented PEEK-ionene + IL composite membranes for CO_2 separations. Thus, the gas (CO_2, N_2, O_2, and CH_4) permeability and diffusivity values of PEEK-ionene + IL composites were determined using a lab-made time-lag apparatus at 20 °C and 2 atm of feed pressure. The permeabilities and permselectivities of PEEK-ionene composite membranes are presented in Table 2, while the gas solubility coefficient values were calculated using Eqn. 1 and both diffusivity and solubility coefficient values are displayed in Table S1.

Table 2. Pure gas permeabilities (P) and permselectivities (α) of PEEK-ionene composite membranes measured at 20 °C and 2 atm of feed pressure.

Membrane Composites	Permeability[a,b]				Permselectivity[b]		
	P_{CO2}	P_{O2}	P_{N2}	P_{CH4}	$\alpha_{CO2/N2}$	$\alpha_{CO2/CH4}$	$\alpha_{O2/N2}$
PEEK[c]	0.96	0.26	0.04	0.03	24.17	31.00	6.5
P1 + 1 eq. IL	5.08 ± 0.08	1.10 ± 0.06	0.61 ± 0.02	0.79 ± 0.07	8.33 ± 0.09	6.44 ± 066	1.58 ± 0.11
P1 + 2 eq. IL	21.0 ± 0.2	1.74 ± 0.21	0.72 ± 0.02	0.85 ± 0.09	28.2 ± 1.9	23.46 ± 0.66	2.19 ± 0.11
P2 + 1 eq. IL	2.76 ± 0.06	0.65 ± 0.04	0.41 ± 0.04	0.43 ± 0.05	6.75 ± 0.09	6.44 ± 0.66	1.59 ± 0.11
P2 + 2 eq. IL	14.7 ± 0.1	1.21 ± 0.02	0.41 ± 0.31	0.59 ± 0.03	35.7 ± 0.7	24.7 ± 1.2	2.94 ± 0.04
P2 + 3 eq. IL	94.5 ± 0.3	8.53 ± 0.53	3.77 ± 0.31	6.02 ± 0.44	26.0 ± 1.0	16.0 ± 0.7	2.26 ± 0.10

[a]Permeability are reported in Barrer, where 1 Barrer = 10^{-10} [cm^3(STP) cm]/(cm^2 s cmHg). [b]Measurements are performed in triplicates. The average and error values for permeabilities and permselectivities were calculated from each individual gas run. [c]The gas permeabilities was adapted from the ref[10]

Similar to glassy poly(IL) and poly(IL)-IL composite membranes, stoichiometric incorporation of "non-polymerizable" IL into the PEEK-ionene membranes has enhanced the gas permeabilities of each individual gas, with a drastic enhancement particularly observed for CO_2 and O_2. For instance, the addition of 1 eq. of free IL to the neat P2 membrane resulted in a well-formed membrane. The gas permeabilities for CO_2, O_2, N_2, and CH_4 are 2.76 ± 0.06, 0.65 ± 0.04, 0.41 ± 0.04, and 0.43 ± 0.05 barrer, respectively (see Table 2). While for P1 + 1 eq. IL composite membranes, a more pronounced increased in gas permeabilities was obtained for 5.08 ± 0.08 (P_{CO2}), 1.10 ± 0.06 (P_{O2}), 0.61 ± 0.02 (P_{N2}), and 0.79 ± 0.07 (P_{CH4}) barrer. The obtained gas permeabilities for PEEK-ionene + IL composites demonstrated excellent performance compared to the conventional PEEK membrane (see Table 2), though the membrane was assessed at different operating conditions (35 °C and 10 atm feed pressure)[10]. Further, incorporation of 2 eq. free IL into the neat PEEK-ionene, the permeability enhanced roughly to 433%, 86%, 0.98%, and 38%, respectively for P2 composite membrane and 314%, 58%, 19%, and 7%, respectively for P1 composite membrane to that of PEEK-ionene + 1 eq. IL composites. But the drastic enhancement of permeabilities was obtained for P2 + 3 eq. IL composite membrane. The permeabilities improved to 3322%, 1212%, 863%, and 1300%, respectively when compared to P2 + 1 eq. IL composite membrane. Examining the permeability data for the PEEK-ionene + IL composites (see Table 2), P2 + 3 eq. IL composite membrane exhibited high CO_2 permeation values largely due to increase in higher free volume spaces generated by inclusion of IL in the dense polymer chain, resulting higher polymer chain mobility. This was further supported by physical properties (density and *d*-spacing) as well as MAS NMR measurements, indicating that the spacer groups, ionic charged units in the structural motif, and the IL loading capacity would affect the gas permeabilities.

In general, the incorporation of free ILs in charged polymers (i.e., ionenes and poly(ILs)) boosts the gas permeabilities due to a significant increase in the diffusivity coefficient.[42, 47-49] To further understand the gas permeation data of PEEK-ionene + IL composites, diffusivities and solubilities coefficients were determined using time-lag apparatus and presented in Table S1. Like gas permeabilities, all gas diffusivities values increased with the addition of IL to the PEEK-ionene membranes. The increase in diffusivity values is primarily attributed to the key modification made in the polymer matrix (spacer length and charge units), *d*-spacing between the polymer units, density, and glass transition. For instance, the CO_2 for P2 composite membranes increased by factors of 3.5 and 13.2 for 2 and 3 eq. of IL, respectively, compared to the P2 + 1 eq. IL composite membranes.

ARTICLE

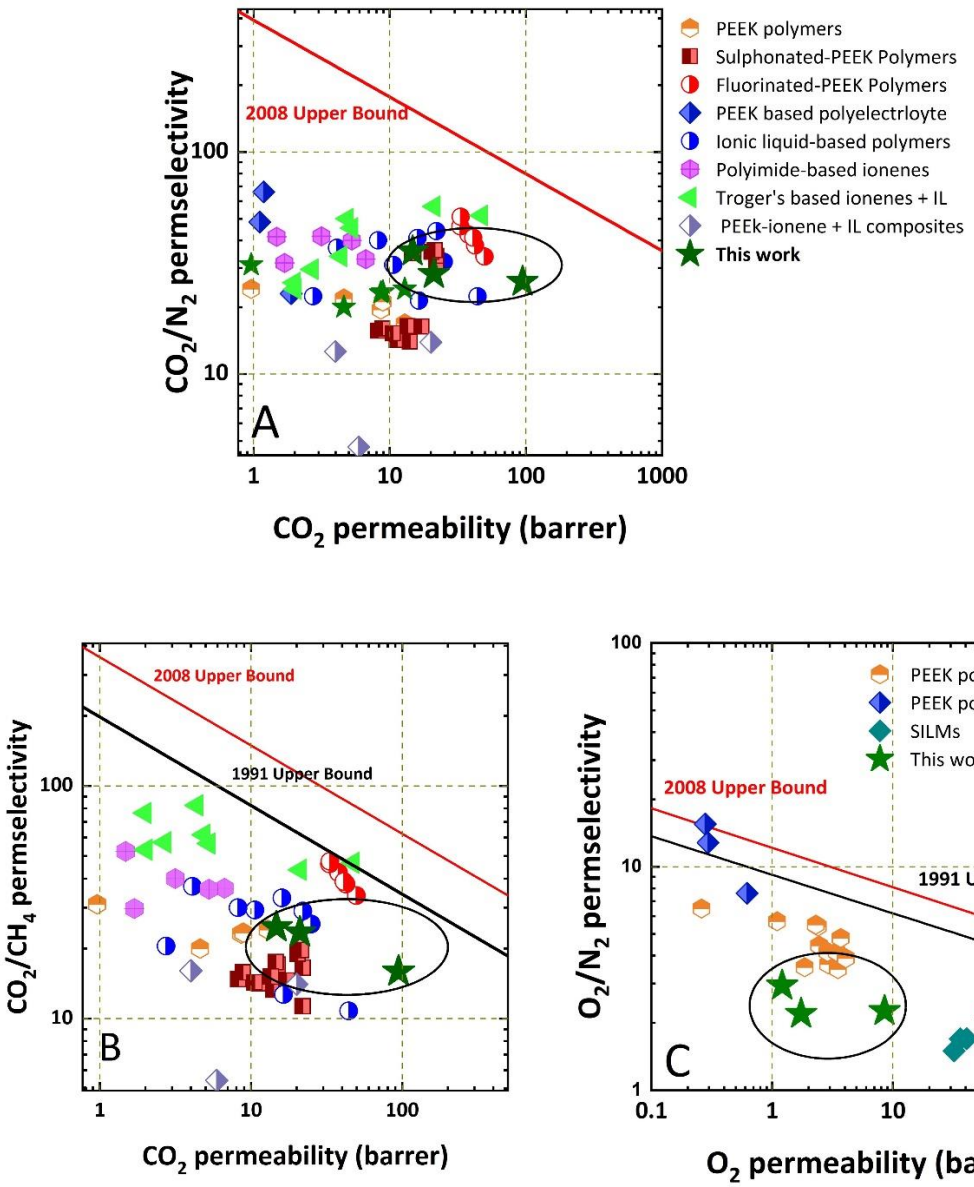

Figure 8. Robeson 1991 and 2008 upper bound plot for comparing the (a) CO_2/N_2, (b) CO_2/CH_4, and (C) O_2/N_2 separation performance of the PEEK-ionene composites. Data take from neat PEEK,[10, 11] modified-PEEK,[20, 29, 50, 51] poly(IL)-IL composites,[48, 52] supported based ILs,[53] imidazolium-based ionenes,[36, 49, 54] and PEEK-ionene + composites[37].

Similarly, the diffusivities values for P1 + 2 eq. IL composite membranes are increased by factors of 3.4 for CO_2, compared to the membrane with 1 eq. of IL present. While the diffusivity of other gas molecules (O_2, N_2, and CH_4) have low coefficient values when compared to smaller gas molecules (CO_2), as the rate of mass transfer per unit area for larger gas molecules are extremely lower compared to CO_2 gas molecules. From the diffusivity data, it is clearly concluded that increasing the amount of IL in the polymers creates more permeable pathways within in the dense matrix and improved the chain mobility of the comonomer segments. The diffusivity values are further

corroborated by the density and *d*-spacing values and a similar trend has been observed in the literature for poly(IL)-IL matrix.[42, 55] Interestingly, the obtained diffusion coefficient results are in contrast with sulfonated-PEEK membranes, where the CO_2 diffusion decreases with the increase in degree of sulfonation.[20]

On the other hand, PEEK-ionene + IL composites exhibited a notable trend in solubility coefficient as the loading capacity increases (see Table S1). This increase in CO_2 solubility compared to the lighter gases is mainly because of higher solubility in ILs caused by stronger interactions between the charged moieties and quadrupolar CO_2 molecules. These results are consistent with number of studies shown in the literature, where the incorporation of IL increases the solubility of CO_2 molecules.[56-58] Interestingly, the solubility coefficient value (see Table S1) decreased after 3 eq. of free IL was included into the P2 polymer. The decreased in CO_2 solubility can be attributed to drastic increase in the diffusivity values for all the gases. Where mobilized IL dramatically increases the FFV space and interacts well with the ionic domains in the dense membrane, could form a highly mobilized material, thereby promoting faster diffusion rates for gases, including CO_2. Similar findings were observed from the solid-state NMR measurements (See Figure 7). Overall, the high permselectivities values for the P2 + 3 eq. IL composite membrane can be attributed to higher diffusion coefficients than a decrease in CO_2 solubility coefficient. On the other hand, the solubility of other gas molecules (O_2, N_2, CH_4) are much lower as compared to CO_2, due to weaker interactions with the ILs. Therefore, the apolar molecules have negligible effect on the solubility coefficient with the IL loading capacity. Besides the relative similar solubilities obtained for each individual gas of P1 + 1 eq. IL and P2 + 1 eq. IL ionenes are not realistic when compared with the ionic polymers, might be due to strong chain-stiffening caused by intermolecular H-bonding or defects present in these two polymeric membranes.

As shown in Table 2, all the PEEK-ionene + IL composite membranes showed the same trend of gas permeabilities: P_{CO2} (3.3 Å) >>> P_{O2} (3.5 Å) >> P_{CH4} (3.8 Å) > P_{N2} (3.6 Å). All the composite membranes exhibited slightly higher CH_4 permeability than that of N_2, which follows in contrast to their kinetic diameters (as shown in parentheses) of the penetrant gas molecules. The increase in permeability of CH_4 over N_2 is mainly arose due to the gas dissolution into the dense membrane. The trend is consistent with the ionene-IL and poly(IL)-IL composite membranes published in the literature.[59-61]

Further it is important to understand the effects of comonomers (aromatic and aliphatic) connectivity and the number charged units between the doubly PEEK segments on the gas transport properties. Both the neat PEEK-ionene polymers with aliphatic and aromatic linkages exhibited poor film-forming capabilities but their flexibility and mechanical stability were greatly enhanced with the free IL loading. Another important observation from Table 2 and Table S1 illustrates that the transport properties are sensitive to the molecular substructures in the main-chain polymer, validates with the *d*-spacing. From the permeation data displayed in Table 2, the gas permeabilities for the P1 membranes are much higher than the P2 membranes and the permeation values increased with IL loading capacity. For instance, CO_2 permeability showed an increase of 184% for P1 + 1 eq. IL to that of P2 + 1 eq. IL composite membrane. This suggests that the mobilized IL plausibly filled more void spaces around the IL sections within the P1 polymeric matrix and strongly interacts with imidazolium moieties in the polymer backbone through electrostatic interactions, which improved chain mobility, thus, enhanced the CO_2 permeability. Surprisingly, as the IL loading capacity increased to 2 eq. IL, the CO_2 permeability differences between these two PEEK-ionene + IL composite membranes with varied connectivity has decreased to 70%. But the results presented in Table 2, clearly indicates that both the composite membranes yield a large increase in the CO_2 permeabilities. For instance, incorporation of free IL into aromatic and aliphatic linker containing PEEK-ionene membranes exhibited 314% and 433% respective increase in CO_2 permeabilities compared to that of respective PEEK-ionene + 1 eq. IL composites. This suggests that higher amounts of free IL loading in both the PEEK-ionene + 2 eq. IL composite membranes significantly increased the free volume and certainly affected the chain flexibility, subsequently enhancing gas permeabilities. However, the xylyl connectivity in PEEK-ionene + 2 eq. IL composite might exhibit stronger π-π interactions, causing less accessible space for the gas molecules to penetrate through the membrane due to effective polymer chain packing, relative to aliphatic containing PEEK-ionene + 2 eq. IL composite. Further, no signs of IL leakage were observed even after adding 3 eq. of IL into the neat P2 membrane. This shows that the presence of aliphatic linkers in PEEK-ionene + IL composite, reduces the intermolecular H-bonding, and increase in charged moieties, esp. bulky Tf_2N counteranions must be accommodated and may cause less effective polymer chain packing, and hence, an enhanced CO_2 permeability was expected with this composition.

To better understand the performance and gas transport data for newly developed PEEK-ionene + IL composite membranes, the CO_2 permeability–selectivity correlations for CO_2/CH_4, CO_2/N_2 and O_2 permeability versus O_2/N_2 gas pairs were appended to Robeson's upper bound plots.[6, 7] As shown in Table 2, as the IL capacity increases in PEEK-ionene membrane, the solubility and diffusivity coefficient of CO_2 are much higher than the other gases, which resulted in excellent CO_2/N_2 and CO_2/CH_4 separations than O_2/N_2 separations. For instance, the incorporation of 2 eq. IL in both the PEEK-ionene + IL composites having xylyl and hexyl groups attached to the imidazolium rings promotes the increase in CO_2/N_2 and CO_2/CH_4 permselectivity. But when the IL content increased to 3 eq., the permselectivities were slightly decreased, due to drastic increase in the permeation and diffusion properties. Overall, P2 + 2 eq. IL composite membrane showed good permselectivity of 35.7 and 24.7 for CO_2/N_2 and CO_2/CH_4, respectively. Here, the IL content is higher than the previously reported PEEK-ionene values[37] and can reach as high as 3 eq., and a substantial increase in gas permeabilities and selectivities is observed. Similarly, an enhanced permeabilities and selectivity (CO_2/N_2) and reduced selectivity for CO_2/CH_4 is observed when compared to the

pristine PEEK polymer[9]. Although, it is difficult to compare the CO_2 performances of newly developed PEEK ionene-IL composites with those from the literature data due to the difference in the polymeric backbone. But still an attempt has been made and the comparative plots were shown in Figure 8. Data from the neutral PEEK,[10, 11] modified-PEEK polymers (sulfonated, fluorinated) and polyelectrolytes,[20, 29, 50, 51] poly(IL)-IL composites,[48, 52] supported IL-membranes,[53] PEEK-ionene + IL composites[37] and other imidazolium-based ionenes[36, 49, 54]. It is known that neutral and substituted PEEK membranes usually demonstrate intrinsic CO_2/N_2 separation properties. Subsequently, the PEEK-ionene + IL composite membranes performed better CO_2/N_2 and CO_2/CH_4 separation than the reported literature values. Even though, the permselectivities fall below the upper bound but the two PEEK-ionene polymers with 2 eq. IL showed better performances than sulphonated-PEEK polymers and within in the range of polar or substituted-PEEK polymers and poly(IL)-IL composites. Interestingly, the P2 + 3 eq. IL exhibited a drastic increase in the permeability (94 Barrer) and CO_2/N_2 permselectivity of 26 due to enhanced diffusivity selectivity compared to mentioned literature values. Both the CO_2/N_2 and CO_2/CH_4 separations are average to better performance when compared to other existing membranes. Subsequently, Figure 8C shows the O_2 permeability versus O_2/N_2 permselectivity values of developed PEEK ionene-IL composites. Although there was not much difference in O_2/N_2 permselectivity values with varying amount of IL, suggests that the current PEEK-ionene + IL composite membranes are less interesting for O_2/N_2 selectivity. Overall, this work shows the innovative polymer designs for gas separation membranes that do not exceed the Robeson upper bound might also lead to new materials that have other applications (e.g., 3D printing, self-healing). Additionally, it's essential to emphasize the uniqueness of our work that neither PEEK or a simple ionene would exhibit independently, like enhanced processability and mechanical strength.

Conclusions

In summary, facile synthetic routes have been employed in the synthesis of imidazole-functionalized PEEK oligomer ($ImK(EEK)_2Im$) and imidazolium-mediated PEEK-ionene containing aromatic and aliphatic linkages. To our knowledge, this is the first example of a "doubly-segmented" ionene, where the neutral and ionic components have more than one repeat unit in each segment. We believe such strategies can be augmented in many ways towards ultimately synthesizing doubly-segmented ionenes with (much) longer segments such as to create condensation polymers that begin to resemble block copolymers.

The doubly-segmented PEEK ionenes in this study have shown potential utility as CO_2 gas separation membranes. These ionenes achieved high molecular weight and displayed moderate solubilities in polar organic solvents when heated, compared to pristine PEEK which has very limited solubility. In comparison to neat PEEK-ionenes, composites containing ILs yield flexible membranes, and their flexibility improved with increasing stoichiometric incorporation of free IL. The thickness for PEEK-ionene + IL composites are in the range of 177–255 μm as prepared by the solution casting method. Interestingly, with the addition of free IL, the structural features of the PEEK-ionenes are modified and that was clearly noticeable in the WAXD spectra and other physical properties. For instance, these newly developed composites exhibited lower densities and higher intersegmental distance due to the presence of IL. Further, MAS-NMR measurements suggested that free IL was concentrated around the IL sections of the main-chain polymer and that molecular interactions are significantly improved with IL loading, resulting highly mobilized materials, thus increasing the CO_2 permeability. The enhancement in permeability is caused by an increase in the diffusion coefficients and solubility coefficients, a property which is characteristic of ILs. Overall, the PEEK-ionene + IL composite membranes showed superior CO_2 permeabilities up to 94 barrer while obtaining moderate CO_2/CH_4 and CO_2/N_2 permselectivities. It is reasonable to suggest that future ionene materials with longer PEEK segments can possess both great mechanical strength and flexibility with great potential for broad applications.

Author Contributions

SR: conceptualization, synthesis, investigation, data curation, characterization, analysis, writing-original draft & editing; CY: data curation, analysis, writing-original draft; KWW, PSS, and AK: data curation; WDE and DJH: supervision, validation, writing-review & editing; JEB: conceptualization, supervision, validation, funding, and writing-review & editing.

ORCID:

SR: 0000-0002-3457-7102
YC: 0000-0001-7417-0991
KWW: 0009-0007-4219-3209
PSS: 0000-0002-1715-6867
AK: 0000-0001-9298-4489
WDE: 0000-0003-3644-5514
DJH: 0000-0002-5529-526X
JEB:0000-0002-8315-2415

Conflicts of interest

There are no conflicts to declare.

Acknowledgements

J.E.B. thank the Major Research Instrumentation (MRI) program of the NSF for the purchase of an NMR spectrometer (CHE-1919906). The authors acknowledge the financial support provided by the U.S. Department of Energy, Office of Science, Basic Energy Sciences, Chemical Sciences, Geosciences, and Biosciences Division, Materials Science and Separation Science programs, FWP 76830.

Notes and references

1. V. Masson-Delmotte, P. Zhai, A. Pirani, S.L. Connors, C. Péan, S. Berger, N. Caud, Y. Chen, L. Goldfarb, M.I. Gomis, M. Huang, K. Leitzell, E. Lonnoy, J. B. R. Matthews, T. K. Maycock, T. Waterfield, O. Yelekçi, R. Yu, and B. Zhou (eds.), *Journal*, 2021, DOI: 10.1017/9781009157896.
2. M. d. E. Joeri Rogelj, Niklas Höhne, Taryn Fransen, Hanna Fekete, Harald Winkler, Roberto Schaeffer, Fu Sha, Keywan Riahi & Malte Meinshausen, *Nature*, 2016, **534**, 631–639.
3. R. Sidhikku Kandath Valappil, N. Ghasem and M. Al-Marzouqi, *J. Ind. Eng. Chem.*, 2021, **98**, 103–129.
4. P. Bernardo, E. Drioli and G. Golemme, *Ind. Eng. Chem. Res.*, 2009, **48**, 4638–4663.
5. R. W. Baker and B. T. Low, *Macromolecules*, 2014, **47**, 6999–7013.
6. L. M. Robeson, *J. Membr. Sci.*, 2008, **320**, 390–400.
7. L. M. Robeson, *J. Membr. Sci.*, 1991, **62**, 165–185.
8. J. C. Jansen and E. Drioli, *Polym. Sci. Ser. A*, 2009, **51**, 1355.
9. D. Shukla, Y. S. Negi, J. S. Uppadhyaya and V. Kumar, *Polymer Rev.*, 2012, **52**, 189–228.
10. Y. P. Handa, J. Roovers and P. Moulinié, *J. Polym. Sci. B Polym. Phys.*, 1997, **35**, 2355–2362.
11. J. M. Mohr, D. R. Paul, G. L. Tullos and P. E. Cassidy, *Polymer*, 1991, **32**, 2387-2394.
12. T. F. Conceição, J. R. Bertolino, G. M. O. Barra and A. T. N. Pires, *Mater. Sci. Eng. C*, 2009, **29**, 575–582.
13. A. Iulianelli and A. Basile, *Int. J. Hydrog. Energy* 2012, **37**, 15241–15255.
14. S. Jiang, H. Sun, H. Wang, B. P. Ladewig and Z. Yao, *Chemosphere*, 2021, **282**, 130817.
15. A. L. Khan, C. Klaysom, A. Gahlaut, X. Li and I. F. J. Vankelecom, *J. Mater. Chem.*, 2012, **22**, 20057−20064.
16. Y. Li and T. S. Chung, *J. Membr. Sci.*, 2008, **308**, 128–135.
17. M. A. Abdulhamid, S.-H. Park, H. Vovusha, F. H. Akhtar, K. C. Ng, U. Schwingenschlögl and G. Szekely, *J. Mater. Chem. A*, 2020, **8**, 24445–24454.
18. A. Parthiban, A. Le Guen, Y. Yansheng, U. Hoffmann, M. Klapper and K. Müllen, *Macromolecules*, 1997, **30**, 2238–2243.
19. M. Puertas-Bartolomé, M. E. Dose, P. Bosch, B. D. Freeman, J. E. McGrath, J. S. Riffle, A. E. Lozano, J. G. de la Campa and C. Álvarez, *RSC Adv.*, 2017, **7**, 55371-55381.
20. A. L. Khan, X. Li, A. Ilyas, M. T. Raza and I. F. J. Vankelecom, *Sep. Purif. Technol.*, 2016, **167**, 1–5.
21. T. U. Rashid, *J. Mol. Liq.*, 2021, **321**, 114916.
22. L. C. Tomé and I. M. Marrucho, *Chem. Soc. Rev.*, 2016, **45**, 2785–2824.
23. X. Yan, S. Gu, G. He, X. Wu and J. Benziger, *J. Power Sources*, 2014, **250**, 90–97.
24. J. Ran, L. Wu, J. R. Varcoe, A. L. Ong, S. D. Poynton and T. Xu, *J. Membr. Sci.*, 2012, **415-416**, 242–249.
25. Q. Hu, Y. Shang, Y. Wang, M. Xu, S. Wang, X. Xie, Y. Liu, H. Zhang, J. Wang and Z. Mao, *Int. J. Hydrog. Energy*, 2012, **37**, 12659–12665.
26. B. Lin, L. Qiu, B. Qiu, Y. Peng and F. Yan, *Macromolecules*, 2011, **44**, 9642–9649.
27. F. Zhang, H. Zhang and C. Qu, *J. Mater. Chem.*, 2011, **21**, 12744–12752.
28. W. Lu, Z.-G. Shao, G. Zhang, Y. Zhao, J. Li and B. Yi, *Int. J. Hydrogen Energy*, 2013, **38**, 9285–9296.
29. I. Kammakakam, H. W. Kim, S. Nam, H. B. Park and T.-H. Kim, *Polymer*, 2013, **54**, 3534–3541.
30. J. E. Bara and K. E. O'Harra, *Macromol. Chem. Phys.* , 2019, **220**, 1900078.
31. J. S. Lee, A. Hocken and M. D. Green, *Mol. Syst. Des. Eng.*, 2021, **6**, 334–354.
32. I. Strużyńska-Piron, M. Jung, A. Maljusch, O. Conradi, S. Kim, J. H. Jang, H.-J. Kim, Y. Kwon, S. W. Nam and D. Henkensmeier, *Eur. Poly. J.*, 2017, **96**, 383–392.
33. R. L. Thankamony, H. Chu, S. Lim, T. Yim, Y.-J. Kim and T.-H. Kim, *Macromol. Res.*, 2015, **23**, 38–44.
34. I. Kammakakam, A. H. N. Rao, H. W. Yoon, S. Nam, H. B. Park and T.-H. Kim, *Macromol. Res.*, 2014, **22**, 907–916.
35. M. S. Mittenthal, B. S. Flowers, J. E. Bara, J. W. Whitley, S. K. Spear, J. D. Roveda, D. A. Wallace, M. S. Shannon, R. Holler, R. Martens and D. T. Daly, *Ind. Eng. Chem. Res.*, 2017, **56**, 5055–5069.
36. I. Kammakakam, K. E. O'Harra, J. E. Bara and E. M. Jackson, *ACS Omega*, 2019, **4**, 3439–3448.
37. K. O'Harra, I. Kammakakam, P. Shinde, C. Giri, Y. Tuan, E. M. Jackson and J. E. Bara, *ACS Appl. Polym. Mater.*, 2022, **4**, 8365−8376.
38. A. Jonas, R. Legras and J. Devaux, *Macromolecules*, 1992, **25**, 5841–5850.
39. H. S. Mehta, Y. Chen, J. A. Sears, E. D. Walter, M. Campos, J. Kothandaraman, D. J. Heldebrant, D. W. Hoyt, K. T. Mueller and N. M. Washton, *Solid State Nucl. Magn. Reson.*, 2019, **102**, 31-35.
40. J. E. Bara, *Ind. Eng. Chem. Res.*, 2011, **50**, 13614–13619.
41. S. Ravula, K. W. Wise, P. S. Shinde and J. E. Bara, *Macromolecules*, 2023, **56**, 6126−6141
42. J. E. Bara, E. S. Hatakeyama, D. L. Gin and R. D. Noble, *Poly. Adv. Technol.*, 2008, **19**, 1415–1420.
43. L. H. Perng, C. J. Tsai and Y. C. Ling, *Polymer*, 1999, **40**, 7321–7329.
44. P. Patel, T. R. Hull, R. W. McCabe, D. Flath, J. Grasmeder and M. Percy, *Polym. Degrad. Stab.*, 2010, **95**, 709–718.
45. D. Aaron and C. Tsouris, *Sep. Sci. Technol.*, 2005, **40**, 321−348.
46. A. A. Yousef Alqaheem, Mari Vinoba, Andrés Pérez, *Int. J. Poly. Sci.*, 2017, **2017**, 1−19.
47. P. Li, K. P. Pramoda and T.-S. Chung, *Ind. Eng. Chem. Res.*, 2011, **50**, 9344–9353.
48. L. C. Tomé, M. A. Aboudzadeh, L. P. N. Rebelo, C. S. R. Freire, D. Mecerreyes and I. M. Marrucho, *J. Mater. Chem. A*, 2013, **1**, 10403–10411.
49. I. Kammakakam, J. E. Bara and E. M. Jackson, *Polym. Chem.*, 2020, **11**, 7370–7381.
50. Y. Zheng, X. Yang, M. Yuan and J. Luo, *High Performance Polymers*, 2019, **31**, 1173–1182.
51. A. L. Khan, X. Li and I. F. J. Vankelecom, *J. Membr. Sci.*, 2011, **372**, 87–96.
52. J. E. Bara, C. J. Gabriel, E. S. Hatakeyama, T. K. Carlisle, S. Lessmann, R. D. Noble and D. L. Gin, *J. Membr. Sci.*, 2008, **321**, 3–7.
53. P. Scovazzo, *J. Membr. Sci.*, 2009, **343**, 199–211.
54. G. P. Dennis, K. E. O'Harra, I. Kammakakam, T. A. Jones, M. S. Mittenthal, B. S. Flowers, Y. Tuan, E. M. Jackson and J. E. Bara, *J. Polym. Sci.* , 2020, **58**, 2664–2674.
55. L. C. Tomé, D. Mecerreyes, C. S. R. Freire, L. P. N. Rebelo and I. M. Marrucho, *J. Membr. Sci.*, 2013, **428**, 260–266.

56. C. Cadena, J. L. Anthony, J. K. Shah, T. I. Morrow, J. F. Brennecke and E. J. Maginn, *J. Am. Chem. Soc.*, 2004, **126**, 5300–5308.
57. M. Klähn and A. Seduraman, *J. Phys. Chem. B*, 2015, **119**, 10066–10078.
58. J. L. Anthony, E. J. Maginn and J. F. Brennecke, *J. Phys. Chem. B*, 2002, **106**, 7315–7320.
59. J. C. Jansen, K. Friess, G. Clarizia, J. Schauer and P. Izák, *Macromolecules*, 2011, **44**, 39–45.
60. M. Klepić, A. Fuoco, M. Monteleone, E. Esposito, K. Friess, P. Izák and J. C. Jansen, *Sep. Purif. Technol.*, 2021, **256**, 117813.
61. L. C. Tomé, M. Isik, C. S. R. Freire, D. Mecerreyes and I. M. Marrucho, *J. Membr. Sci.*, 2015, **483**, 155–165.

ARTICLE